

# Self-organization of charged particles on a 2D lattice subject to anisotropic Jahn-Teller-type interaction and 3D Coulomb repulsion

T. Mertelj<sup>1,2</sup>, V.V. Kabanov<sup>1,3</sup>, J. Miranda<sup>1</sup> and D. Mihailovic<sup>1,2</sup>

<sup>1</sup>*Jozef Stefan Institute, Jamova 39, 1000 Ljubljana, Slovenia*

<sup>2</sup>*Faculty of Mathematics and Physics, University of Ljubljana, Slovenia and*

<sup>3</sup>*Department of Physics, Loughborough University, Loughborough LE11 3TU, UK*

(Dated: January 9, 2018)

Self-organization of charged particles on a 2D lattice, subject to an anisotropic Jahn-Teller-type interaction and 3D Coulomb repulsion is investigated. In the mean-field approximation without Coulomb interaction, the system displays a phase transition of first order. In the presence of the Coulomb repulsion the global phase separation becomes unfavorable and the system shows a mesoscopic phase separation, where the size of the charged regions is determined by the competition between the ordering energy and the Coulomb energy.

The phase diagram of the system as a function of particle density and temperature is obtained by systematic Monte Carlo simulations. With decreasing temperature a crossover from a disordered state to a state composed from mesoscopic charged clusters is observed. In the phase separated state charged clusters with even number of particles are more stable than those with odd number of particles in a large range of particle densities. With increasing particle density at low temperatures a series of crossovers between states with different cluster sizes is observed. Above half filling in addition to the low temperature clustering another higher temperature scale, which corresponds to orbital ordering of particles, appears.

We suggest that the diverse functional behaviour - including superconductivity - observed in transition metal oxides can be thought to arise from the self-organization of this type.

PACS numbers:

## I. INTRODUCTION

The presence of nanoscale inhomogeneities is ubiquitous in the cuprate superconductors[3, 4, 5, 6, 7], the magnetoresistive manganites[8, 9, 10, 11, 12, 13] and other doped transition metal oxides[14, 15, 16]. Furthermore, there is emerging consensus that doped charge carriers in the oxides may phase segregate to form nanoscale textures. These are believed to be of importance for achieving their functional properties such is superconductivity in the cuprates[7] and giant magnetoresistance in the manganites[17].

For the cuprates the idea of charge segregation appeared soon after the discovery of superconductivity [18, 19, 20]. In a doped semiconductor the phase separation may have two different origins. The first is the chemical origin and is associated with the segregation of dopant atoms. This type of phase segregation is usually temperature independent and weakly dependent on external perturbation. Exceptions may appear due to a large mobility of dopant atoms at relatively high temperature.

If the mobility of impurity atoms is small one might expect a pure electronic mechanism of phase separation. In this case the electronic system is in thermodynamic equilibrium and competing phases are close in energy. This is typical for the systems exhibiting a first order phase transition. Electronic phase separation is very often observed in the magnetic semiconductors like *EuSe* or *EuTe* [21, 22, 23]. Therefore the idea of the charge segregation in the cuprate superconductors and in the manganites is very often associated with magnetic degrees of

freedom [24, 25, 26], where the phase separation is discussed within  $t - J$  model. In Refs. [27, 28, 29, 30] phase separation was studied within Hubbard model. The results are still controversial. In some cases the  $t - J$  model displays clear static [24] or dynamic[25] phase separation. The situation is quite different for the Hubbard model. For example the results of numerical simulations[30] suggest that the phase separation is absent at any set of parameters and for any size of the lattice. Nevertheless, all these models do not consider *long-range* Coulomb repulsion which has very strong effect on the phase separation. [20, 31, 32, 33, 34, 35, 36]

The long-range Coulomb repulsion together with the surface energy determine the topology of the two phase state. The charged carriers have the tendency towards spatial segregation which is caused by the fact that the free energy density of the phase with finite density of carriers is lower than the free energy density of the undoped system. On the other hand, the charge segregation leads to the charging effect because the dopant atoms are distributed uniformly in the system. Therefore, a strong electric field appears which has tendency to mix the charged phases. In the low doping limit there is a low concentration of charged droplets and they do not overlap. The system behaves as an insulator. When the concentration increases the percolative transition to a new phase is expected[17, 37, 38].

More recently it was suggested that an interplay of a short range lattice attraction and the long-range Coulomb repulsion could lead to the formation of short metallic or insulating strings of polarons[39, 40]. This was mainly motivated by observation of giant isotope ef-

fect in manganites and cuprates[41, 42]. In ref. [43] we suggested that an anisotropic mesoscopic Jahn-Teller interaction between electrons and  $k \neq 0$  optical phonons might lead to the formation of carrier pairs and stripes. A slightly different approach, based on elasticity was considered more recently for the case of the manganites by Kugel and Khomskii [44] using the methods of Eremin et al.[45], and by Shenoy et al.[46].

The fundamental question which we try and answer here is how charged particles order in the presence of anisotropic Jahn-Teller type interaction, particularly when their density becomes large. We consider charged particles on a 2D square lattice subject to *only* the long-range Coulomb interaction and an anisotropic Jahn-Teller (JT) deformation. In the preliminary report we have considered a narrow doping range, but have found a clear evidence of phase segregation and preferential formation of pairs.[33] Here we extend this study over the full doping range.

In the mean field (MF) approximation without Coulomb repulsion, the system displays a first order phase transition to an ordered state below some critical temperature. In the presence of Coulomb repulsion global phase separation becomes unfavorable and the system shows a mesoscopic phase separation, where the size of charged regions is determined by the competition between the ordering energy and the Coulomb energy. Using Monte-Carlo (MC) simulations we show that the system can form many different mesoscopic textures, such as clusters and stripes, depending only on the magnitude of the Coulomb repulsion compared to the anisotropic lattice attraction and the density of charged particles. Surprisingly, in agreement with previous report a feature arising from the anisotropy introduced by the Jahn-Teller interaction is that in a wide part of the phase diagram objects with even number of particles are found to be more stable than with odd number particles, which could be significant for superconductivity when tunnelling is included[37].

## II. FORMULATION

The model proposed in the ref.[43] involves all interactions allowed by the symmetry. We consider a simplified version of the model, where only the interaction leading to the deformation of the  $B_{1g}$  symmetry is taken into account. The interaction with  $B_{2g}$  mode leads to similar effects and therefore for our purposes we can restrict ourselves by consideration  $B_{1g}$  mode only. As a result the interacting part of the Hamiltonian has the form:

$$H_{JT} = g \sum_{\mathbf{r}, \mathbf{l}} \sigma_{3,1} \{ (r_x^2 - r_y^2) f_0(r) \} (b_{\mathbf{l}+\mathbf{r}}^\dagger + b_{\mathbf{l}+\mathbf{r}}), \quad (1)$$

here the Pauli matrix  $\sigma_{3,1}$  describes two components of the electronic doublet, and  $f_0(r)$  is a symmetric function describing the range of the interaction. We omit the spin index in the sum, since we ignore spin structure at

present. The resulting model could be easily reduced to a lattice gas model. This is performed using the Lang-Firsov transformation or equivalently the adiabatic approximation for the phonon field. Let us introduce the classical variable  $\Phi_{\mathbf{i}} = (b_{\mathbf{i}}^+ + b_{\mathbf{i}})/\sqrt{2}$  and minimize the energy as a function of  $\Phi_{\mathbf{i}}$  in presence of the harmonic term  $\omega \sum_{\mathbf{i}} \Phi_{\mathbf{i}}^2/2$ . We obtain the deformation, which corresponds to the minimum energy,

$$\Phi_{\mathbf{i}}^{(0)} = -\sqrt{2}g/\omega \sum_{\mathbf{r}} \sigma_{3,\mathbf{i}+\mathbf{r}} f(\mathbf{r}), \quad (2)$$

where  $f(\mathbf{r}) = (r_x^2 - r_y^2)f_0(r)$ . Substituting  $\Phi_{\mathbf{i}}^{(0)}$  to the Hamiltonian (1) and taking into account that the carriers are charged we arrive to the lattice gas model. To formulate the model we use a pseudospin operator  $S$  with  $S = 1$  to describe the occupancies of the two electronic levels  $n_1$  and  $n_2$ . Here  $S^z = 1$  corresponds to the state with  $n_1 = 1$ ,  $n_2 = 0$ ,  $S_i^z = -1$  to  $n_1 = 0$ ,  $n_2 = 1$  and  $S_i^z = 0$  to  $n_1 = n_2 = 0$ . Simultaneous occupancy of both levels is excluded due to the high onsite Coulomb repulsion (CR) energy. The Hamiltonian in terms of the pseudospin operator is given by

$$H_{JT-C}^{LG} = \sum_{\mathbf{i}, \mathbf{j}} (V_i(\mathbf{i} - \mathbf{j}) S_i^z S_j^z + V_c(\mathbf{i} - \mathbf{j}) Q_i Q_j), \quad (3)$$

where  $Q_{\mathbf{i}} = (S_{\mathbf{i}}^z)^2$ .  $V_c(\mathbf{m}) = e^2/\epsilon_0 a m$  is the Coulomb potential,  $e$  is the charge of electron,  $\epsilon_0$  is the static dielectric constant and  $a$  is the effective unit cell period. The anisotropic short range attraction potential is given by

$$V_l(\mathbf{m}) = g^2/\omega \sum_{\mathbf{i}} f(\mathbf{i}) f(\mathbf{m} + \mathbf{i}). \quad (4)$$

The attraction in this model is generated by the interaction of electrons with optical phonons. The radius of the attraction force is determined by the radius of the electron-phonon interaction and the dispersion of the optical phonons[40].

A similar model can be formulated in the limit of the continuous media. In this case the deformation is characterized by components of the strain tensor. For the two dimensional case we can define 3 components of the strain tensor:  $e_1 = u_{xx} + u_{yy}$  transforming as the  $A_{1g}$  representation of the  $D_{4h}$  group,  $\epsilon = u_{xx} - u_{yy}$  transforming as the  $B_{1g}$  representation and  $e_3 = u_{xy}$  transforming as the  $B_{2g}$  representation. These components of the tensor are coupled linearly with the two-fold degenerate electronic state which transforms as the  $E_g$  or  $E_u$  representation of the point group. Similarly to the case of interaction with optical phonons we will keep the interaction with deformation of the  $B_{1g}$  symmetry, namely  $\epsilon$  only. The Hamiltonian without the Coulomb term has the form:

$$H = \tilde{g} \sum_{\mathbf{i}} S_{\mathbf{i}}^z \epsilon_{\mathbf{i}} + \frac{1}{2} (A_1 e_{1,\mathbf{i}}^2 + A_2 \epsilon_{\mathbf{i}}^2 + A_3 e_{3,\mathbf{i}}^2) \quad (5)$$

here  $A_j$  are corresponding components of the elastic modulus tensor, and  $\tilde{g}$  is coupling constant of the charge carriers with the strain tensor. The components of the strain tensor are not independent [46] and obey the compatibility condition:

$$\nabla^2 e_1(\mathbf{r}) - 4\partial^2 e_3(\mathbf{r})/\partial x \partial y = (\partial^2/\partial x^2 - \partial^2/\partial y^2)\epsilon(\mathbf{r}).$$

The compatibility condition leads to the long range anisotropic interaction between polarons. To derive the Hamiltonian we minimize Eq.(5) with respect to  $e_1$  and  $e_3$  taking into account compatibility condition. The resulting Hamiltonian in the reciprocal space has the form:

$$H = \tilde{g} \sum_{\mathbf{k}} S_{\mathbf{k}}^z \epsilon_{\mathbf{k}} + (A_2 + A_1 U(\mathbf{k})) \frac{\epsilon_{\mathbf{k}}^2}{2}. \quad (6)$$

The wavevector dependence of the potential is given by

$$U(\mathbf{k}) = \frac{(k_x^2 - k_y^2)^2}{k^4 + 8(A_1/A_3)k_x^2 k_y^2}. \quad (7)$$

By minimizing the energy with respect to  $\epsilon_{\mathbf{k}}$  and including the long-range CR we again obtain Eq.(3). The anisotropic interaction potential  $V_l(\mathbf{m}) = -\sum_{\mathbf{k}} \exp(i\mathbf{k} \cdot \mathbf{m}) \frac{\tilde{g}^2}{2(A_2 + A_1 U(\mathbf{k}))}$  is determined in this case by the interaction with the classical deformation and is long-range as well. It decays as  $1/r^2$  at large distances. Since attraction forces decay faster than the Coulomb repulsion at large distances the attraction can overcome the Coulomb repulsion at short distances leading to the mesoscopic phase separation.

Irrespective of whether the resulting interaction between polarons is generated by acoustic or optical phonons the main physical picture remains the same. In both cases there is an anisotropic attraction between polarons over short distances. This interaction can be either ferromagnetic or antiferromagnetic in terms of the pseudospin operators depending on the spatial direction. Without losing generality we assume that  $V(\mathbf{m})$  is nonzero only for the nearest neighbors and can be either ferromagnetic or antiferromagnetic.

### III. MEAN FIELD

Our main goal is to study this lattice gas model (3) at a constant average density,

$$n = \frac{1}{N} \sum_{\mathbf{i}} Q_{\mathbf{i}}, \quad (8)$$

where  $N$  is the total number of sites. However, to clarify the physical picture we first perform calculations in absence of long-range CR at a fixed chemical potential first by adding the term  $-\mu \sum_{\mathbf{i}} Q_{\mathbf{i}}$  to the Hamiltonian (3).

Similar models were studied many years ago on the basis of the molecular-field approximation in the Bragg-Williams formalism [47, 48]. The mean-field equations

for the two variables  $n$  and  $M = \frac{1}{N} \sum_{\mathbf{i}} S_{\mathbf{i}}^z$  have the form[47]:

$$M = \frac{2 \sinh(2zV_l M/k_B T)}{\exp(-\mu/k_B T) + 2 \cosh(2zV_l M/k_B T)}, \quad (9)$$

$$n = \frac{2 \cosh(2zV_l M/k_B T)}{\exp(-\mu/k_B T) + 2 \cosh(2zV_l M/k_B T)} \quad (10)$$

here  $z = 4$  is the number of the nearest neighbours for the square lattice in 2D and  $k_B$  is the Boltzman constant. For positive  $\mu > 0$  equation (9) has 2 solutions below  $T_c$ . The solution with  $M = 0$  is unstable while the solution with a finite  $M$  corresponds to the global minimum with  $n \rightarrow 1$  for  $T \rightarrow 0$ . When  $-2zV_l < \mu < 0$  the equation has 3 solutions below  $T_{c1} < T_c$ . The free energy has two minima and one maximum. The phase transition at  $T_{c1}$  is of first order. The trivial solution  $M = 0$  corresponds to the case when  $n \rightarrow 0$  as  $T \rightarrow 0$ . For  $\mu < -2zV_l$  there is only the trivial solution of the equation  $M = 0$ .

When the number of particles is fixed (Eq.(8)) the system is unstable with respect to global phase separation below  $T_{crit}(n)$ . The line of the phase transition is determined by the condition:  $F(M = 0, \mu_{crit}(T), T) = F(M(T), \mu_{crit}(T), T)$  where  $F$  is the free energy,  $\mu_{crit}(T)$  is the critical chemical potential and  $M$  is the solution of Eq. (9). As a result, at a fixed average  $n$  two phases with  $n_0(T) = n(M = 0, \mu_{crit}(T), T)$  and  $n_M(T) = n(M(T), \mu_{crit}(T), T)$  coexist as determined by Equations(9,10). The region of phase coexistence is shown in Fig.1. For comparison with the MF solutions we performed Monte-Carlo simulations of the model Eq.(3) in absence of the Coulomb forces. Due to strong fluctuations in 2D the critical temperature determined from MC simulations is reduced by factor of  $\sim 2$  in comparison to the MF result.

### IV. COULOMB FRUSTRATED FIRST ORDER PHASE TRANSITION

Let us now consider the role of the Coulomb repulsion. The area under the  $T_{crit}(n)$  in Fig.1 is the area of phase coexistence. If we fix the temperature the two phases with the bulk concentrations  $n_0$  and  $n_M$  will have volume fractions  $1 - x$  and  $x$  respectively, where  $x = (n - n_0)/(n_M - n_0)$ . Since the system is globally electroneutral, the phases with  $n_0$  and  $n_M$  are charged. However, to break electroneutrality requires a large increase of the Coulomb energy. As a consequence growth of charged regions with two different charge densities is blocked by the Coulomb forces.

In the literature there are a few examples of introduction of charging effects in the problem of phase separation [33, 34, 35, 36]. There are several different possibilities to include long-range Coulomb forces in the model. Muratov[36] proposed that the order parameter is a charged scalar and the charge density is proportional

to the order parameter. This situation is similar to the problem of a charged Bose gas in magnetic field considered in [49]. Similar situation is considered in Ref.[35] where the free energy has two distinct minima as a function of the density and gradient terms in the free energy are replaced by the surface tension. Jamei, Kivelson and Spivak [34] considered the case with a scalar order parameter where the charge density is coupled to the order parameter as an external field.

In our case, symmetry allows coupling of the charge density with square of the order parameter only. Let us consider the classical free energy density corresponding to the first order phase transition:

$$F_1 = ((t - 1) + (\eta^2 - 1)^2)\eta^2. \quad (11)$$

Here  $t = (T - T_c)/(T_0 - T_c)$  is the dimensionless temperature. At  $t = 4/3$  ( $T = T_0 + (T_0 - T_c)/3$ ) a nontrivial minimum in the free energy appears. At  $t = 1$  ( $T = T_0$ ) the first order phase transition occurs. Below  $t = 1$  the trivial solution  $\eta = 0$  corresponds to the metastable phase. At  $t = 0$  ( $T = T_c$ ) the trivial solution becomes unstable. In order to study the case of the Coulomb frustrated phase transition we have to add coupling of the order parameter to the local charge density. In our case the order parameter describes the sublattice orbital magnetization and therefore only square of the order parameter can be coupled to the local charge density  $\rho$ :

$$F_{coupl} = -\alpha\eta^2\rho. \quad (12)$$

The proposed free energy functional is similar to that proposed in the Ref. [34]. In our case the charge plays a role of the local temperature, while in Ref.[34] there is a linear coupling of the charge to the order parameter and the charge density plays a role of the external field.

The total free energy density should also contain the gradient term and the electrostatic energy:

$$F_{grad} + F_{el} = C(\nabla\eta)^2 + \frac{1}{2}K[\rho(\mathbf{r}) - \bar{\rho}] \int d\mathbf{r}' [\rho(\mathbf{r}') - \bar{\rho}]|\mathbf{r} - \mathbf{r}'|. \quad (13)$$

Here we write  $\bar{\rho}$  explicitly to take into account global electroneutrality. The total free energy Eqs.(11,12,13) should be minimized at fixed  $t$  and  $\bar{\rho}$ .

Next, we proceed to show that the Coulomb term leads to phase separation in 2D. Minimization of  $F$  with respect to the charge density  $\rho(\mathbf{r})$  leads to the following equation:

$$-\alpha\nabla_{3D}^2\eta^2 = 4\pi K[\rho(\mathbf{r}) - \bar{\rho}]\delta(z), \quad (14)$$

here we write explicitly that electrostatic field is 3D but the charge density  $\rho(\mathbf{r})$  is confined in the 2D plane ( $z = 0$ ) and depends only on 2D vector  $\mathbf{r}$ . To preserve correct dimensionality we introduce the layer thickness  $d$ . We believe that this condition is favorable for creating charge segregation because electrostatic field is not screened in

the third direction. Solving this equation by applying the Fourier transform and substituting the solution back into the free energy density we obtain:

$$F = F_1 - \alpha\eta^2\bar{\rho} + C(\nabla\eta)^2 - \frac{\alpha^2}{8\pi^2 Kd} \int d\mathbf{r}' \frac{\nabla(\eta(\mathbf{r})^2)\nabla(\eta(\mathbf{r}')^2)}{|\mathbf{r} - \mathbf{r}'|}. \quad (15)$$

As a result the free energy functional is similar to the case of first order phase transition with a shifted critical temperature due to presence of the term  $\alpha\eta^2\bar{\rho}$  and with additional nonlocal gradient term.

To demonstrate that the uniform solution has a higher free energy then a nonhomogeneous solution we make the Fourier transformation of the gradient term:

$$F_{grad} \propto Ck^2|\eta_{\mathbf{k}}|^2 - \frac{\alpha^2 k|(\eta^2)_{\mathbf{k}}|^2}{4\pi Kd}, \quad (16)$$

where  $\eta_{\mathbf{k}}$  and  $(\eta^2)_{\mathbf{k}}$  are Fourier components of the order parameter and square of the order parameter respectively. If we assume that the solution is uniform i.e.  $\eta_0 \neq 0$  and  $(\eta^2)_0 \neq 0$  small nonuniform corrections to the solution reduce the free energy at small  $\mathbf{k}$ , where the second term dominates.

The situation is different in 3D. Direct solution of the equation for the charge density leads to the *local* gradient term of higher order  $-\frac{\alpha^2}{8\pi K}(\nabla\eta(\mathbf{r})^2)^2$ . This term can also lead to instability and higher order expansion in gradient terms become important.

## V. MONTE CARLO SIMULATIONS

To substantiate above arguments we performed Monte-Carlo (MC) simulations of the system described by the Hamiltonian Eq.(3) with and without the presence of the long-range CR. The simulations were performed on a square lattice with dimensions  $L \times L$  sites with  $10 \leq L \leq 100$  at different dimensionless temperatures  $t = k_B T \epsilon_0 a / e^2$ . The short range potential  $v_l(\mathbf{i}) = V_l(\mathbf{i})\epsilon_0 a / e^2$  was taken to be nonzero only for  $|\mathbf{i}| < 2$  and was therefore specified by two parameters:  $v_l(1, 0)$  and  $v_l(1, 1)$ . To further minimize the number of free parameters only the nearest neighbors attractive interaction potential  $v_l(1, 0)$  was taken to be nonzero in most cases presented here.

We first performed MC simulations of the model at a constant chemical potential in the absence of CR. Due to presence of first order phase transition, the particle density probability distribution  $P_{t,\mu}(n)$  has two peaks when the chemical potential is near the critical value  $\mu_{crit}(t)$ . At  $\mu_{crit}(t)$  the two peaks have equal height corresponding to the densities of the two coexisting phases,  $n_0$  and  $n_M$ . A standard Metropolis algorithm[50] in combination with simulated annealing[51] and histogram reweighting technique[56] gave reliable results only at higher temperatures near maximum  $t_{crit}(n)$ . To improve reliability at lower temperatures we used a variant of multicanonical

approach[57] adapted to uniformly sample states over the full range of densities[58],  $n$ , at a constant dimensionless temperature  $t_{sim}$  and chemical potential  $\mu_{sim}$ . At each temperature the final histogram acquisition run involved at least  $10^6$  MC pseudospin flips per site. The density probability histograms  $P_{t_{sim},\mu}(n)$  for several values of the chemical potential  $\mu$  close to the simulation chemical potential  $\mu_{sim}$  were then calculated at each  $t_{sim}$  by reweighting [56] (see Fig. 2). From the histogram with equal peak heights the densities of the two coexisting phases  $n_0$  and  $n_M$  were then determined at given  $t_{sim}$ .

In simulations at constant  $n$  one MC step consisted from a single update per each particle, where the trial move consisted from setting  $S_z = 0$  at the site with nonzero  $Q_i$  and  $S_z = \pm 1$  at a randomly selected site with zero  $Q_i$ . A standard Metropolis algorithm [50] in combination with simulated annealing[51] was used in this case. A typical simulated annealing run consisted from a sequence of MC simulations at different temperatures. At each temperature equilibration phase consisting from  $10^3 - 10^6$  MC steps was first executed followed by the averaging phase consisting from the same or greater number of MC steps. Observables were measured after each averaging MC step during the averaging phase only.

At constant  $n$  in absence of the CR global phase separation below  $t_{crit}(n)$  occurs in the form of a large cluster with  $M \neq 0$ . To detect onset of clustering we measure the nearest neighbor density correlation function (CF)  $g_{\rho L} = \frac{1}{4n(1-n)L^2} \sum_{|\mathbf{m}|=1} \langle \sum_i (Q_{i+\mathbf{m}} - n)(Q_i - n) \rangle_L$ , where  $\langle \rangle_L$  represents the MC average. We define the temperature  $t_{cl}(n)$  at which  $g_{\rho L}$  rises to 50% of its low temperature value (see Fig. 1b) as the characteristic crossover temperature related to the formation of clusters.

In Fig. 1a we show the results of MC simulations in absence of the Coulomb repulsion. We find that for  $n \gtrsim 0.4$  the boundary conditions strongly affect the  $t_{crit}(n)$  line calculated at the constant chemical potential. When we use open boundary conditions (OBC)  $t_{crit}(n)$  is strongly suppressed above  $n \approx 0.4$  in comparison to the result obtained with the periodic boundary conditions (PBC). At constant  $n$ , on the other hand, the influence of the boundary conditions on  $t_{cl}(n)$  is less pronounced. The  $t_{cl}(n)$  calculated with both types of boundary conditions closely follow the  $t_{crit}(n)$  line calculated with PBC. Above  $n \approx 0.6$   $t_{cl}(n)$  for OBC is only slightly higher than for PBC. We attribute insensitivity of  $t_{cl}(n)$  to boundary conditions at fixed  $n$  to sensitivity of the correlation function to the short range correlations which are less sensitive to boundary conditions.

Next we analyze the model in the presence of the long-range CR at constant  $n$ . In Fig. 3 we show a typical temperature dependence of the average energy per particle estimator  $\langle e_{MC} \rangle_L$  for different system sizes  $L$  in presence of the long range CR using OBC. Error bars represent the standard deviation  $\sigma_{e_{MC}} = \sqrt{\langle e_{MC}^2 \rangle_L - \langle e_{MC} \rangle_L^2}$ . The average energy monotonously drops with decreasing tem-

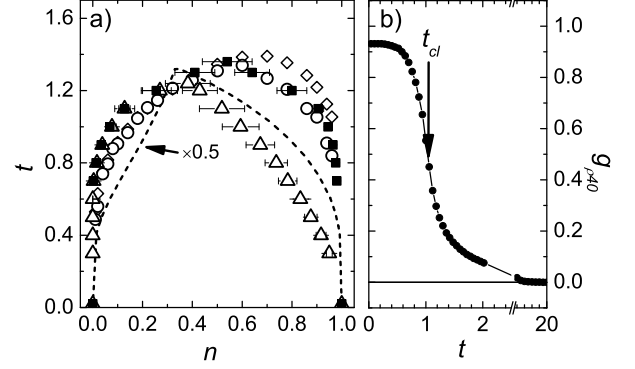


FIG. 1: (a) The phase diagram of the model in absence of the Coulomb repulsion. The dashed line represents the mean field (MF) solution. The full squares (■) represent the  $t_{crit}(n)$  line calculated for the periodic boundary conditions by means of the multicanonical MC algorithm with the system of size  $L = 40$ . For comparison the  $t_{crit}(n)$  line is shown (△) for open boundary conditions. The  $t_{cl}(n)$  lines for periodic (□) and open (◇) boundary conditions are also shown. (b) The dependence of the nearest neighbor density correlation function,  $g_{\rho L}$ , on temperature in absence of the Coulomb repulsion. The definition of  $t_{cl}(n)$  is indicated by arrow. The numerical errorbars are of the order of symbol sizes

perature. The drop is more pronounced in the temperature interval  $\sim 0.5 > t > \sim 0.1$  in which clusters start to form. Below  $t \sim 0.1$  the clusters are partially ordered. The temperature dependence of  $\langle e_{MC} \rangle_L$  is virtually identical for all  $L$  (We should note that the curves are vertically shifted by 0.1 for clarity.) indicating that the boundary effects on  $\langle e_{MC} \rangle_L$  are negligible even for the smallest system sizes.

To check reliability of our simulations we analysed MC update dynamics by calculating the autocorrelation function of energy fluctuations,

$$g_{eL}(\tau_{MC}) = \frac{1}{K\sigma_{e_{MC}}^2} \sum_{i=1}^K (e_{MC}(i + \tau_{MC}) - \langle e_{MC} \rangle_L)(e_{MC}(i) - \langle e_{MC} \rangle_L), \quad (17)$$

where  $e_{MC}(i)$  represents the energy per site at  $i$ -th MC step and  $\tau_{MC}$  represents the MC time. A typical time dependence of  $g_{eL}(\tau_{MC})$  is shown in the inset in Fig. 4. The autocorrelation function drops with the characteristic MC relaxation time  $\tau_R$ .  $1/\tau_R$  displays Arrhenius temperature dependence (see Fig. 4) down to the temperature where clusters start to order. Below this temperature  $\tau_R$  behaves more erratically. The activation energy strongly depends on the magnitude of the short range potential  $v_l(1, 0)$ .

In the temperature region where clusters partially order the heat capacity  $c_L = \partial \langle e_{MC} \rangle_L / \partial t$  displays the

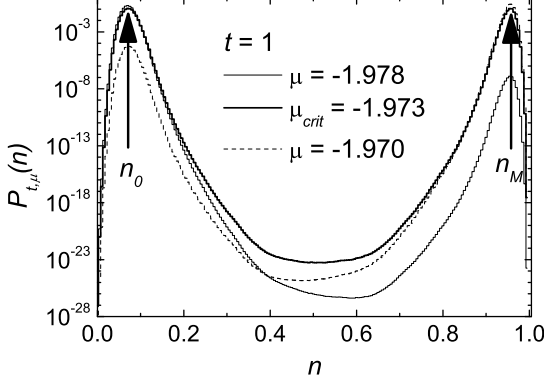


FIG. 2: Histograms of the density probability distribution  $P_{t,\mu}(n)$  at the chemical potential near  $\mu_{crit}(t)$  obtained by multicanonical MC simulation in absence of Coulomb repulsion. The values of the coexisting densities  $n_0$  and  $n_M$  at the given temperature are indicated by arrows. Note the logarithmic scale.

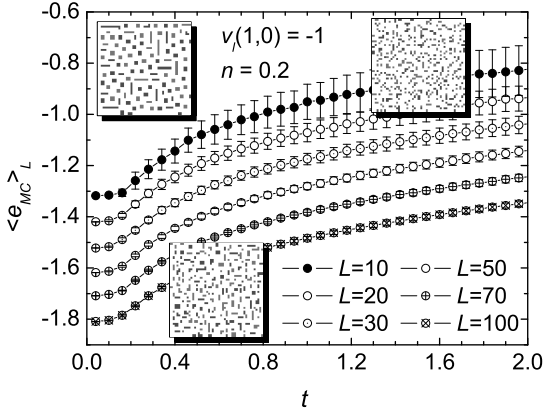


FIG. 3: A typical temperature dependence of the average energy per particle estimator  $\langle e_{MC} \rangle_L$  for different system sizes  $L$ . Insets show snapshots of particle distribution at different temperatures, where darker and brighter shades of grey represent  $S_i^z = 1$  and  $-1$  respectively. Curves are vertically shifted for 0.1, error bars represent  $\sigma_{e_{MC}}$ .

peak at  $t_{co}(n)$  (see Fig. 5b). The peak displays no scaling with  $L$  indicating that no long range ordering of clusters appears. Inspection of the particle distribution snapshots at low temperatures[33] reveals that finite size domains form (see Fig. 6). Within the domains the clusters are ordered. The domain wall dynamics seems to be much slower than our MC simulation timescale preventing domains to grow. The effective  $L$  is therefore limited by the domain size. This explains the absence of the scaling and clear evidence for a phase transition near  $t_{co}(n)$ . From the simulations it is therefore not clear whether the absence of complete cluster ordering is due to the finiteness of the

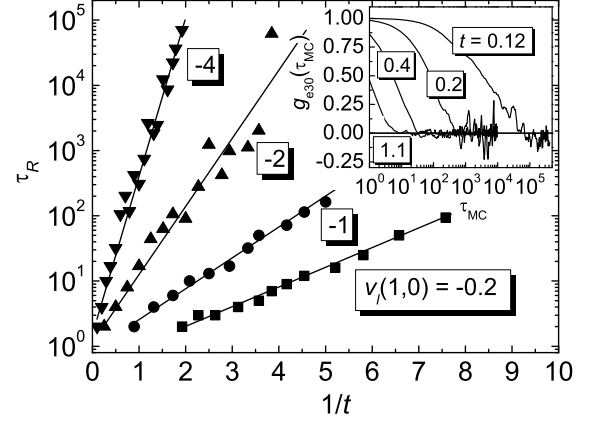


FIG. 4: The characteristic MC relaxation time  $\tau_R$  as a function of temperature for different values of  $v_l(1,0)$ . Thin lines represent the Arrhenius fits. The inset shows the autocorrelation function  $g_{e30}(\tau_{MC})$  at a few temperatures for  $v_l(1,0) = -1$ . For convenience  $\tau_R$  is defined as a value of  $\tau_{MC}$  where  $g_{eL}(\tau_{MC}) = 0.25$ .

MC simulation or it is also due to the glassy form of the free energy landscape. The square shape of the sample may frustrate the cluster orders with nontetragonal symmetries, while practically achievable number of MC steps per temperature step warrant reliable MC averages only above the temperature which is of the same order as  $t_{co}(n)$ . The cluster ordering temperature  $t_{co}(n)$  which is the lowest energy scale at all densities is only weakly  $n$ -dependent between  $0.1 \lesssim n \lesssim 0.9$ .

We now focus on the short range potential shape which promotes formation of stripes[33]. We set  $v_l(1,0) = -1$  and  $v_l(1,1) = 0$  and study the dependence of clustering on particle density. To detect clustering we again use the nearest neighbour CF. In Fig. 5c we plot a typical nearest neighbor CF,  $g_{\rho 40}(1,0)$ , as a function of temperature. At high temperatures  $t \gg |v_l(1,0)|$  CF is slightly negative due to the long range CR. When the temperature decreases CF becomes positive and further rises with the decreasing temperature. No saturation of CF as in the case of absence of the CR forces is observed with the decreasing temperature (see Fig. 1b). Again we define the temperature at which CF rises to 50% of its low temperature value as the characteristic crossover temperature,  $t_{cl}(n)$ , related to the formation of clusters. The dependence of  $t_{cl}(n)$  on the particle density is shown in Fig. 5a for different boundary conditions. While in absence of the long-range CR  $t_{cl}(n)$  closely follows the  $t_{crit}(n)$  line (Fig 1a), suppression of clustering by the CR forces results in a significant decrease of  $t_{cl}(n)$ .

Different boundary conditions influence  $t_{cl}(n)$  only for densities above  $n \gtrsim 0.5$ . In this region the particles that form clusters are holes ( $Q_i = 0$ ) in the background of pseudospins ( $Q_i = 1$ ). The open boundary conditions are effectively a perimeter formed from holes which attracts

T. Mertelj et al. Fig. 5

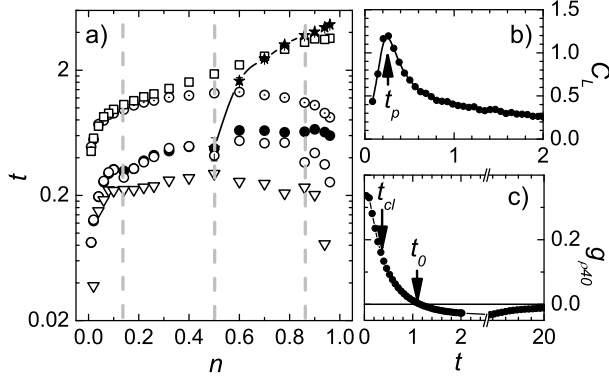


FIG. 5: (a) The phase diagram of the model in presence of the long range Coulomb repulsion. Open circles ( $\circ$ ) and full circles ( $\bullet$ ) represent the  $t_{cl}(n)$  line for periodic and open boundary conditions respectively while dotted circles ( $\odot$ ) represent the  $t_{cl}(n)$  line for periodic boundary conditions in absence of the long range CR. The onset of clustering,  $t_0(n)$  is shown by open squares ( $\square$ ) and the cluster ordering temperature  $t_{CO}(n)$  by open triangles ( $\triangle$ ). The pseudospin (orbital) ordering temperature is shown by full stars ( $\star$ ). Note the logarithmic scale. The error-bars are of the order of symbol sizes or smaller.

T. Mertelj et al. Fig. 6

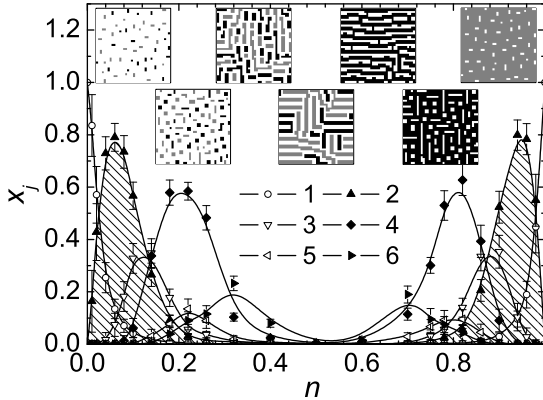


FIG. 6: The density dependence of the cluster-size distribution function  $x_j$  for a few smallest cluster sizes as a function of the average density at the temperature  $t = 0.14$ . The regions of densities where pairs prevail are shadowed.

holes and by pinning enhances hole clustering resulting in an increase of  $t_{cl}(n)$  for OBC.

In addition for  $n \geq 0.5$  and our choice of  $v_l(\mathbf{i})$  the pseudospin background ferromagnetically orders at  $t_S(n)$  which increases with increasing density as shown in Fig. 5a. The pseudospin ordering temperature is significantly higher than  $t_{cl}(n)$ . Despite this the particle-hole symmetry of the  $t_{cl}(n)$  line is absent. The absence of the particle-hole symmetry is a consequence of different entropy contributions of doubly degenerate particle level

( $S_{iz} = \pm 1$  for  $Q_i = 1$ ) and singly degenerate hole level ( $S_{iz} = 0$  for  $Q_i = 0$ ).

The  $t_{cl}(n)$  line does not appear smooth. There are clear dips at  $n \approx 0.14$ ,  $n = 0.5$  and  $n \approx 0.86$ . With increasing density the ground state of the system apparently goes through a series of crossovers related to the most probable cluster sizes as shown in Fig. 6. While the dip at half filling clearly corresponds to commensurate ordering of stripes the other two dips approximately correspond to the densities at which clusters of size four start to replace pairs (see Fig. 6.). There is no obvious commensuration to underlying lattice at these densities. At densities at which larger clusters start to replace fours no comparable anomaly is observed in the  $t_{cl}(n)$  line.

Despite the presence of the CR forces some clusters already start to form at temperatures higher than  $t_{cl}(n)$ . We can estimate the upper limit for the onset of cluster formation by the temperature,  $t_0(n)$ , at which  $g_{pL}(1, 0)$  crosses 0. It is interesting that  $t_0(n)$  almost coincides with the  $t_{crit}(n)$  line (see Fig. 5a) below  $n \lesssim 0.4$  while at higher densities the onset of clustering appears at much higher temperatures. In the region  $0.5 < n \lesssim 0.75$  the onset of clustering is higher in temperature than the pseudospin ordering temperature  $t_S(n)$  while above  $n \approx 0.75$  the pseudospin ordering represents the highest energy scale.

To get further insight in the cluster formation we measured the cluster-size distribution function. In Fig. 6 we show the low temperature density dependency of the cluster-size distribution function,  $x_j = N_p(j)/(nL^2)$ , where  $N_p(j)$  is the number of particles for  $n \leq 0.5$  or holes for  $n > 0.5$  in clusters of size  $j$ . At the highest temperature  $x_j$  is close to the distribution expected for the random ordering. When the temperature decreases the number of larger clusters starts to increase at the expense of the single particle number.[33] Further down in temperature depending on the average density  $n$  clusters of a certain size start to prevail at the expense of all other sizes. Depending on the particle density prevailing clusters can be pairs up to  $n \approx 0.14$ , quadruples up to  $n \approx 0.3$  etc.. The situation is qualitatively symmetrical for the clusters formed by holes at  $n > 0.5$ . We should note that for the given  $v_l(1, 0)$  the system prefers clusters with an even number of particles, however different  $v_l(i, j)$  might lead to the preference for an odd number of particles in a cluster.

It should also be emphasized that the preference to certain cluster sizes becomes clearly apparent only at temperatures lower than  $t_{cl}(n)$ , however the transition is not abrupt but gradual with decreasing temperature. This is seen also from gradual increase of the average cluster size with decreasing temperature shown in Fig. 7. Around half filling the average cluster size starts to diverge at low temperatures indicating formation of long stripe-like objects (see insets in Fig. 6) and proximity of the percolation.

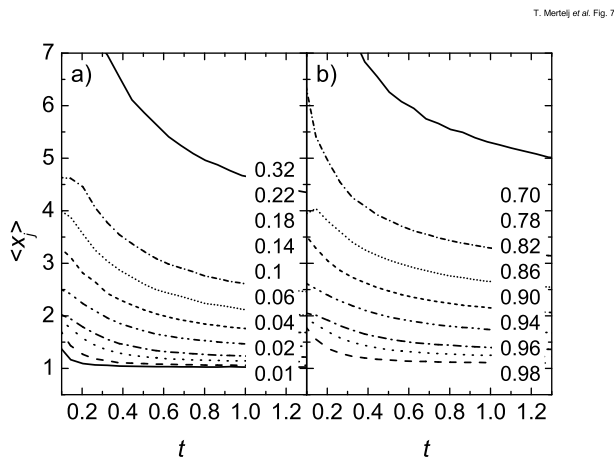


FIG. 7: The temperature dependence of the average cluster size for different particle densities  $n$  below half filling (particle clusters) (a) and above half filling (hole clusters) (b).

## VI. CONCLUSIONS

We presented the results of extensive investigation of the ordering of charged Jahn-Teller polarons as a function of doping and temperature. We consider charged particles on a 2D square lattice subject to *only* the long-range Coulomb interaction and an anisotropic Jahn-Teller (JT) deformation.

We prove that without the long-range Coulomb repulsion the system is unstable with respect to the first order phase transition below the density dependent critical temperature. This was demonstrated by the solution of the mean field equation as well as by direct Monte Carlo

simulations. It was shown that this result does not depend on the type of boundary conditions and the error due to finite size effect is estimated.

In the presence of the Coulomb repulsion the global phase separation becomes unfavorable and the system shows a mesoscopic phase separation, where the size of the charged regions is determined by the competition between the ordering energy and the Coulomb energy. The phenomenological theory of this effect was formulated where the square of the order parameter is coupled with the charge density. The charge density plays the role of the local temperature. This type of coupling is more general in comparison with the models where the charge plays the role of an external field.

Using Monte-Carlo (MC) simulations we showed that below a characteristic clustering temperature the system forms many different mesoscopic textures, such as clusters and stripes, depending only on the magnitude of the Coulomb repulsion compared to the anisotropic lattice attraction and the density of charged particles. Below the clustering temperature the system goes through a series of crossovers between phases with different mesoscopic textures when the particle density is increased. The low temperature part of the phase diagram is rather symmetric with respect to half filling. However, above half doping another high temperature scale appears corresponding to orbital ordering of the particles. Surprisingly, a feature arising from the anisotropy introduced by the Jahn-Teller interaction is that objects with an even number of particles more stable than those with an odd number of particles. Such a behaviour could have significant implications for superconductivity when tunnelling is included[37].

- 
- [1] E.Dagotto, Rep.Mod.Phys. **66**, 763 (1994)
  - [2] J. Jaklic and P. Prelovšek, Adv. Phys. **49**, 1 (2000).
  - [3] R.J.McQueeney et al, Phys. Rev. Lett, **82**, 628 (1999).
  - [4] A.Bianconi et al Phys.Rev.Lett **76** 3412 (1996), Bozin et al., Phys.Rev.Lett. **84**, 5856 (2000).
  - [5] S.H.Pan et al., Nature **413**, 282 (2001), McElroy et al., Nature **422**, 592 (2003).
  - [6] J.Demsar et al, Phys. Rev. Lett. **82**, 4918 (1999), see also review by D.Mihailovic and V.V.Kabanov in "Superconductivity", ACS series on Structure and Bonding. Eds. A.Bussmann-Holder and K.A.Müller, (2004). , cond-mat/0407204
  - [7] see also: D.Mihailovic and K.A.Müller, in High  $T_c$  Superconductivity 1996: Ten years after the discovery. Eds. E.Kaldis, E.Liarokapis and K.A.Müller, NATO ASI, Ser. E. Vol. 343 (Kluwer, 1997) p. 243.
  - [8] J.M. De Teresa, M.R. Ibarra, P.A. Algarabel, C. Ritter, C. Marquina, J. Blasco, J. García, A. del Moral, and Z. Arnold, Nature (London) **386**, 256 (1997).
  - [9] G. Allodi, R. De Renzi, G. Guidi, F. Licci, and M. W. Pieper, Phys. Rev. B **56**, 6036 (1997).
  - [10] M. Uehara, S. Mori, C. H. Chen, and S.-W. Cheong, Nature (London) **399**, 560 (1999).
  - [11] M. Fath, S. Freisem, A.A. Menovsky, Y. Tomioka, J Aarts, JA Mydosh, Science **285**, 1540 (1999).
  - [12] G. Papavassiliou, M. Fardis, M. Belesi, T. G. Maris, G. Kallias, M. Pissas, D. Niarchos, C. Dimitropoulos, and J. Dolinsek, Phys. Rev. Lett. **84**, 761 (2000).
  - [13] Y. Kawasaki, T. Minami, Y. Kishimoto, T. Ohno, K. Zenmyo and H. Kubo T. Nakajima and Y. Ueda, Phys. Rev. Lett. **96**, 037202 (2006).
  - [14] P. L. Kuhns, M. J. R. Hoch, W. G. Moulton, A. P. Reyes, J. Wu, and C. Leighton, Phys. Rev. Lett. **91**, 127202 (2003).
  - [15] M.H. Sage, G.R. Blake, G.J. Nieuwenhuys, T. T. M. Palstra, Phys. Rev. Lett. **96**, 036401 (2006).
  - [16] S.-W. Cheong, H. Y. Hwang, C. H. Chen, B. Batlogg, L. W. Rupp, Jr., and S. A. Carter, Phys. Rev. B **49**, 7088 - 7091 (1994).
  - [17] E. Dagotto, T. Hotta, A. Moreo, Physics Reports, **344**, 1 (2001).
  - [18] J. Zaanen, O Gunnarsson, Phys. Rev. B, **40**, 7391 (1989).
  - [19] V.J. Emery, S. Kivelson and O.Zachar, Phys.Rev.B **56**, 6120 (1997).



- [20] L.P. Gorkov, A.V. Sokol, Pisma ZhETF, **46**, 333 (1987); L.P. Gorkov, J. Supercond., **14**, 365, (2001).
- [21] J. Vitins, P. Wachter, Phys. Rev. B **12**, 3829, (1975).
- [22] Y. Shapira, S. Foner, N. Oliveira, T. Reed, Phys. Rev. B, **5**, 2674 (1972).
- [23] Y. Shapira, S. Foner, N. Oliveira, Phys. Rev. B, **10**, 4765 (1974).
- [24] V.J.Emery, S.A.Kivelson, H. Lin, Phys. Rev. Lett. **64**, 475 (1990)
- [25] V.J.Emery, S.A.Kivelson, Physica C, **209**, 597 (1993).
- [26] G. Uhrig, R. Vlaming Phys. Rev. Lett., **71**, 371 (1993).
- [27] A. Angelucci, S. Sorella Phys. Rev. B, **47**, 8858 (1993).
- [28] A. Singh, Z. Tesanovic, J. Kim, Phys. Rev. B, **44**, 7757 (1991).
- [29] Y. Bang, G. Kotliar, C. Castellani, et al, Phys. Rev. B, **43**, 13724 (1991).
- [30] A. Moreo, D. Scalapino, E. Dagotto, Phys. Rev. B, **43**, 11442 (1991)
- [31] U.Löw, V.J.Emery, K.Fabricious, S.A.Kivelson, Phys. Rev.Lett.**72**,1918 (1994).
- [32] J. Lorenzana, C. Castellani, and C. Di Castro, Phys. Rev. B, **64**, 235127 (2001); Europhys. Lett. **57**, 704 (2002).
- [33] T. Mertelj, V. V. Kabanov, D. Mihailovic, Phys. Rev. Lett. **94**, 147003 (2005).
- [34] R. Jamei, S. Kivelson, and B. Spivak, Phys. Rev. Lett., **94**, 056805 (2005).
- [35] C Ortix, J. Lorenzana, C. Di Castro, Phys. Rev. B, **73**, 245117 (2006).
- [36] C.B. Muratov, Phys. Rev. E, **66**, 066108 (2002).
- [37] D.Mihailovic, V.V.Kabanov and K.A.Muller, Europhys. Lett. **57**, 254 (2002).
- [38] A.S. Alexandrov, A.M. Bratkovsky, and V.V. Kabanov, Phys. Rev. Lett., **96**, 117003 (2006).
- [39] F.V. Kusmartsev, Phys. Rev. Lett., **84**, 530, (2000), *ibid* **84**, 5026 (2000).
- [40] A.S. Alexandrov, V.V. Kabanov Pisma ZhETF, **72**, 825 (2000) (JETP letters, **72**, 569 (2000)).
- [41] G.M. Zhao, K. Conder, H. Keller, K.A. Muller, Nature, **381**, 676 (1996).
- [42] G.M. Zhao, M.B. Hunt, H. Keller, K.A. Muller, Nature, **385**, 236 (1997).
- [43] D. Mihailovic, V.V. Kabanov, Phys. Rev., B, **63**, 054505, (2001); V.V. Kabanov, D. Mihailovic, Phys. Rev., B, **65**, 212508, (2002), V.V.Kabanov and D.Mihailovic, J.Superc. **13**, 959 (2000).
- [44] D.I. Khomskii, K.I. Kugel, Europhys. Lett. **55**, 208 (2001); Phys. Rev. B, **67**, 134401 (2003).
- [45] M.B. Eremin, A.Yu. Zavidonov, B.I. Kochelaev, ZhETF, **90**, 537 (1986).
- [46] S.R. Shenoy, T. Lookman, A. Saxena, A.R. Bishop, Phys. Rev. B, **60**, R12537 (1999); T. Lookman, et al, Phys. Rev. B, **67**, 024114 (2003); K.H. Ahn, T. Lookman, A.R. Bishop, Nature **428**, 401 (2004).
- [47] J. Lajzerovicz, J. Sivardiere, Phys. Rev. A **11**, 2079 (1975).
- [48] J. Sivardiere, J. Lajzerovicz, Phys. Rev. A **11**, 2090 (1975)
- [49] V.V. Kabanov, A.S. Alexandrov, Phys. Rev. B, **71**, 132511 (2005).
- [50] N. Metropolis, et al. *J. Chem. Phys.* **21**, 1087 (1953).
- [51] S. Kirkpatrick, C.D. Gelatt and M.P. Vecchi, Science **220** (1983) 671-680.
- [52] E.M.Lifshitz and L.P.Pitaevski, Physical Kinetics, ch.12 (Butterworth-Heinemann, 1980).
- [53] T.Mertelj et al. (to be published).
- [54] D.Reagor et al., Phys.Rev.Lett. **62**, 2048 (1989).
- [55] A.S.Alexandrov and N.F.Mott "Polarons and Bipolarons", (World Scientific, 1995).
- [56] A. M. Ferrenberg and R. H. Swendsen, *Phys. Rev. Lett.* **61**, 2635 (1988).
- [57] B. A. Berg, T. Neuhaus, Physics Letters B **267**, 249 (1991).
- [58] G. Orkoulas and A. Z. Panagiotopoulos, J. Chem. Phys. **110**, 1581 (1999).